

# Quadratic Spline Methods for the Shallow Water Equations on the Sphere: Galerkin

Anita T. Layton<sup>1,\*</sup>, Christina C. Christara<sup>2,†</sup>, and Kenneth R. Jackson<sup>2,†</sup>

<sup>1</sup>*Department of Mathematics, University of North Carolina, Chapel Hill, North Carolina, USA.*

<sup>2</sup>*Department of Computer Science, University of Toronto, Toronto, Ontario, Canada.*

E-mail: <sup>1</sup>layton@amath.unc.edu, <sup>2</sup>{ccc, krj}@cs.toronto.edu

## Abstract

Currently in most global meteorological applications, low-order finite difference or finite element methods, or the spectral transform method are used. The spectral transform method, which yields high-order approximations, requires Legendre transforms. The Legendre transforms have a computational complexity of  $\mathcal{O}(N^3)$ , where  $N$  is the number of subintervals in one dimension, and thus render the spectral transform method unscalable. In this study, we present an alternative numerical method for solving the shallow water equations (SWEs) on a sphere in spherical coordinates. In this implementation, the SWEs are discretized in time using the two-level semi-Lagrangian semi-implicit method, and in space on staggered grids using the quadratic spline Galerkin method. We show that, when applied to a simplified version of the SWEs, the method yields a neutrally stable solution for the meteorologically significant Rossby waves. Moreover, we demonstrate that the Helmholtz equation arising from the discretization and solution of the SWEs should be derived algebraically rather than analytically, in order for the method to be stable with respect to the Rossby waves. These results are verified numerically using Boyd's equatorial wave equations [2] with initial conditions chosen to generate a soliton.

*Keywords:* numerical weather prediction; finite element; semi-Lagrangian semi-implicit; Rossby stability; staggered grids.

---

\*Part of this work was done while the author was at the Department of Computer Science, University of Toronto and published as her doctoral thesis [18].

†Partly supported by Natural Sciences and Engineering Research Council (NSERC) of Canada.

*Subject classifications:* 65N30; 76B65; 86A10.

## 1 Introduction

Weather prediction is a science with a long history. Its objective is the description and prediction of the behaviour of the atmosphere, ocean water and sea ice. The accuracy of weather prediction depends on many factors, such as the accuracy of the knowledge of the state of the atmosphere at the initial time, the numerical methods applied, and the resolution used in these methods. Because weather prediction computations are time-consuming, there is interest among the scientific community in developing accurate and efficient methods for weather prediction. One way to achieve high accuracy in weather prediction computations is to consider high-order discretization methods.

The spatial discretization schemes that are commonly used in meteorological simulations are finite difference schemes, spectral schemes, and finite element schemes. For instance, the models used by the National Center for Atmospheric Research (NCAR) and the European Centre for Medium-Range Weather Forecasts (ECMWF) are based on the spectral transform method [9, 19, 20], while the model developed by the Canadian Meteorological Centre in partnership with the Meteorological Research Branch (CMC-MRB) uses a variable-resolution cell-integrated finite element scheme [4, 5]. Although the spectral transform method is popular and offers superior accuracy at a sufficiently high resolution, the efficiency of the method at high resolutions is reduced, because the cost of performing spectral transforms increases rapidly with spatial resolution. In the case of Fourier transforms in the longitudinal direction, fast Fourier Transforms (FFTs) may be used and their computational cost grows as  $\mathcal{O}(N^2 \log(N))$ , where  $N$  is the number of spatial subintervals in one dimension. However, an efficient method for performing Legendre transforms, analogous to FFTs, has not yet been developed. Thus, the Legendre transforms in the latitudinal direction are often performed by summation and their costs escalate at a rate of  $\mathcal{O}(N^3)$ . Therefore, finite element methods will likely offer a competitive alternative in the future, since, compared to the spectral transform method, their computational complexity grows at a slower rate. Pro-

vided that a sufficiently efficient solver is applied for the solution of the linear system arising from the Helmholtz problem, the computational costs of finite difference and finite element methods applied to the shallow water equations (SWEs) on the sphere increase quadratically with the number of gridpoints in one dimension (i.e.,  $\mathcal{O}(N^2)$ ). Moreover, finite element methods can incorporate adaptive grids and, compared to spectral methods, are more suitable for massively parallel computers.

In this paper and in a companion paper [11], we present finite element-based numerical methods for the SWEs in spherical coordinates. The SWEs, which describe the inviscid flow of a thin layer of fluid in two dimensions [8], have been used for many years by the atmospheric modeling community to test promising numerical methods for solving atmospheric and oceanic problems. Because the earth is approximately spherical, most global atmospheric models in use today are based on spherical coordinates. To define the equations on the sphere, let  $u$  and  $v$  be the wind velocity components in the  $\lambda$  (longitudinal) and  $\theta$  (latitudinal) directions, respectively, and  $\phi$  be the geopotential. Let  $R$  be the radius of the earth,  $\Omega$  its rotational speed, and  $f = 2\Omega \sin \theta$  the Coriolis parameter, where  $R$  and  $\Omega$  are assumed to be constant. In spherical coordinates, the SWEs are given by

$$\frac{du}{dt} - \left( f + \frac{u \tan \theta}{R} \right) v + \frac{\phi_\lambda}{R \cos \theta} = 0, \quad (1)$$

$$\frac{dv}{dt} + \left( f + \frac{u \tan \theta}{R} \right) u + \frac{\phi_\theta}{R} = 0, \quad (2)$$

$$\frac{d\phi}{dt} + \frac{\phi}{R \cos \theta} [u_\lambda + (v \cos \theta)_\theta] = 0, \quad (3)$$

where the Lagrangian derivative is defined by

$$\frac{d}{dt} \equiv \frac{\partial}{\partial t} + \frac{u}{R \cos \theta} \frac{\partial}{\partial \lambda} + \frac{v}{R} \frac{\partial}{\partial \theta}, \quad (4)$$

and the subscripts  $\lambda$  and  $\theta$  denote the spatial derivatives in the two directions. Since  $u$  and  $v$  are multi-valued at the poles, we adopt the approach of Côté and Staniforth [7] and compute the components of the wind images instead:  $U \equiv u \cos \theta / R$  and  $V \equiv v \cos \theta / R$ . Thus, we solve the following equations, obtained by multiplying the motion equations (1)–(2) and the continuity equation (3) by  $\cos \theta / R$  and  $\cos \theta$ , respectively,

expressing the resulting equations in terms of  $U$  and  $V$ , and isolating the nonlinearity in the continuity equation (3) in a logarithmic term

$$\frac{dU}{dt} - fV + \frac{\phi_\lambda}{R^2} = 0, \quad (5)$$

$$\frac{dV}{dt} + fU + \frac{\cos \theta}{R^2} \phi_\theta + \delta = 0, \quad (6)$$

$$\cos \theta \frac{d}{dt} \log \phi + \left[ \frac{U_\lambda}{\cos \theta} + V_\theta \right] = 0, \quad (7)$$

where  $\delta \equiv (U^2 + V^2) \sin \theta / \cos^2 \theta$ .

Along the longitude, functions are assumed periodic, whereas at the poles ( $\theta = \pm\pi/2$ ), homogeneous Dirichlet boundary conditions are imposed on the wind image components:  $U(\lambda, \pm\pi/2) = V(\lambda, \pm\pi/2) = 0$ . The latitudinal boundary conditions on  $\phi$  are designed to mimic the behaviour of its spherical harmonic expansions [7], and are set to be homogeneous Neumann:  $\phi_\theta(\lambda, \pm\pi/2) = 0$ .

In this paper, the SWEs are discretized in time using the two-level semi-Lagrangian semi-implicit (SLSI) method, and in space using the quadratic spline Galerkin (QSG) method. In the companion paper [11], the optimal quadratic spline collocation (OQSC) methods are used for the spatial discretization. Our numerical results show that QSG methods, when applied in conjunction with the SLSI method, is stable and non-dispersive for the meteorologically significant Rossby waves, that the method exhibits locally fourth-order spatial convergence, and that the method compares favorably to the linear spline Galerkin method, which forms the basis of the method in [3].

## 2 Time Discretization

Discretization schemes based on a semi-Lagrangian treatment of advection have generated considerable interest in the past decade for the efficient integration of atmospheric models, since they offer the promise of larger timestep size, with no loss in accuracy when compared to the Eulerian-based advection schemes, in which the timestep size is limited by more severe stability restrictions [15, 16].

A semi-Lagrangian time discretization scheme in spherical coordinates approximates the Lagrangian derivative along particle trajectories defined by the velocity vec-

tor with components  $d\lambda/dt = u/(R \cos \theta)$  and  $d\theta/dt = v/R$ . Let  $(\delta\lambda^{n+1}, \delta\theta^{n+1})$  be the displacement of a fluid particle in the time interval  $t_n$  to  $t_{n+1}$ , ending at the downstream point  $(\lambda, \theta)$  at  $t_{n+1}$ . We adopt the two-level scheme which approximates a function on a trajectory originating at the upstream departure point  $(\lambda - \delta\lambda^{n+1}, \theta - \delta\theta^{n+1})$  and terminating at  $(\lambda, \theta)$ . For an arbitrary function  $\psi(\lambda, \theta, t)$ , let  $\tilde{\psi}^n$  denote the corresponding upstream function for the time interval  $t_n$  to  $t_{n+1}$ . That is, for the downstream gridpoint  $(\lambda, \theta)$  associated with the displacement  $(\delta\lambda^{n+1}, \delta\theta^{n+1})$

$$\tilde{\psi}^n(\lambda, \theta) \equiv \psi(\lambda - \delta\lambda^{n+1}, \theta - \delta\theta^{n+1}, t_n). \quad (8)$$

The Lagrangian derivative in the interval  $t_n$  to  $t_{n+1}$  is approximated by

$$\frac{d\tilde{\psi}^{n+\frac{1}{2}}}{dt} \approx \frac{\psi^{n+1} - \tilde{\psi}^n}{\Delta t}. \quad (9)$$

If the fast gravity terms were treated explicitly, they would severely restrict the timestep even with semi-Lagrangian advection approximations. Thus, to obtain maximum benefit from the semi-Lagrangian approach, one may combine the semi-Lagrangian approximations with semi-implicit approximations. A semi-implicit treatment of the gravity and Coriolis terms implies that a function is averaged in time along particle trajectories:

$$\tilde{\psi}^{n+\frac{1}{2}} \approx \frac{\psi^{n+1} + \tilde{\psi}^n}{2}. \quad (10)$$

When discretized in time using the two-level SLSI scheme, the SWEs take the form

$$\frac{U^{n+1} - \tilde{U}^n}{\Delta t} - \frac{\tilde{f}^{n+\frac{1}{2}}}{2}(V^{n+1} + \tilde{V}^n) + \frac{1}{2R^2}(\phi_\lambda^{n+1} + \tilde{\phi}_\lambda^n) = 0, \quad (11)$$

$$\frac{V^{n+1} - \tilde{V}^n}{\Delta t} + \frac{\tilde{f}^{n+\frac{1}{2}}}{2}(U^{n+1} + \tilde{U}^n) + \frac{\cos \tilde{\theta}^{n+\frac{1}{2}}}{2R^2}(\phi_\theta^{n+1} + \tilde{\phi}_\theta^n) + \tilde{\delta}^{n+\frac{1}{2}} = 0, \quad (12)$$

$$\cos \tilde{\theta}^{n+\frac{1}{2}} \left( \frac{\log \phi^{n+1} - \log \tilde{\phi}^n}{\Delta t} \right) + \frac{1}{2} \left[ \left( \frac{U_\lambda^{n+1} + \tilde{U}_\lambda^n}{\cos \tilde{\theta}^{n+\frac{1}{2}}} \right) + (V_\theta^{n+1} + \tilde{V}_\theta^n) \right] = 0. \quad (13)$$

Functions at time-level  $t_{n+1}$  are evaluated at gridpoints  $(\lambda_l, \theta_m)$ ; those at time-level  $t_{n+\frac{1}{2}}$  are evaluated at approximate trajectory midpoints  $(\lambda_l - \delta\lambda_l^{n+1}/2, \theta_m - \delta\theta_m^{n+1}/2)$ ; and those at time-level  $t_n$ , called the ‘‘upstream functions,’’ are evaluated at approximate departure points  $(\lambda_l - \delta\lambda_l^{n+1}, \theta_m - \delta\theta_m^{n+1})$ . For notational simplicity, let  $\tilde{f} \equiv \tilde{f}^{n+\frac{1}{2}}$  and  $\tilde{\theta} \equiv \tilde{\theta}^{n+\frac{1}{2}}$ . The trajectories are computed according to the algorithm described by

Côté and Staniforth [6]. The departure points usually fall between gridpoints and spatial interpolation is required to obtain function values at departure points. Cubic polynomial interpolation gives fourth-order spatial truncation errors with very little damping [1], and is thus the method of choice in our implementation.

To solve the time discretized SWEs (11)–(13), the equations are first discretized in space, and then the wind images  $U$  and  $V$  are eliminated from the system to yield a nonlinear Helmholtz equation for the geopotential  $\phi$  only. To this end, we move the  $\phi_\lambda^{n+1}$  and  $\phi_\theta^{n+1}$  terms of the motion equations (11) and (12) to the right side and then rewrite the resulting equations in matrix form

$$\begin{aligned} \begin{bmatrix} U^{n+1} \\ V^{n+1} \end{bmatrix} + \left(\frac{\Delta t}{2R^2}\right) \begin{bmatrix} c & d \\ -d & c \end{bmatrix} \begin{bmatrix} \phi_\lambda^{n+1} \\ \cos \tilde{\theta} \phi_\theta^{n+1} \end{bmatrix} \\ = \begin{bmatrix} a & b \\ -b & a \end{bmatrix} \begin{bmatrix} \tilde{U}^n \\ \tilde{V}^n \end{bmatrix} - \left(\frac{\Delta t}{2R^2}\right) \begin{bmatrix} c & d \\ -d & c \end{bmatrix} \begin{bmatrix} \tilde{\phi}_\lambda^n \\ \cos \tilde{\theta} \tilde{\phi}_\theta^n + 2R^2 \tilde{\delta}^{n+\frac{1}{2}} \end{bmatrix} \equiv \begin{bmatrix} \tilde{R}_u^n \\ \tilde{R}_v^n \end{bmatrix}, \end{aligned} \quad (14)$$

where  $a$ ,  $b$ ,  $c$ , and  $d$  are functions of  $\theta$  defined by

$$a = \frac{1 - z^2}{1 + z^2}, \quad b = \frac{2z}{1 + z^2}, \quad c = \frac{1}{1 + z^2}, \quad d = \frac{z}{1 + z^2}, \quad \text{where } z = \frac{\Delta t \tilde{f}}{2}. \quad (15)$$

We also rewrite (13) as

$$\begin{aligned} \cos \tilde{\theta}^{n+\frac{1}{2}} \log \phi^{n+1} + \frac{\Delta t}{2} \left( \frac{U_\lambda^{n+1}}{\cos \tilde{\theta}^{n+\frac{1}{2}}} + V_\theta^{n+1} \right) \\ = \cos \tilde{\theta}^{n+\frac{1}{2}} \log \tilde{\phi}^n - \frac{\Delta t}{2} \left( \frac{\tilde{U}_\lambda^n}{\cos \tilde{\theta}^{n+\frac{1}{2}}} + \tilde{V}_\theta^n \right) \equiv \tilde{R}_\phi^n. \end{aligned} \quad (16)$$

### 3 Space Discretization

To apply the QSG method to the time-discretized SWEs, we first define two uniform partitions along the longitude,

$$\begin{aligned} \Delta_\lambda &\equiv \{0 = \lambda_0 < \lambda_1 < \dots < \lambda_{N_\lambda} = 2\pi\} \text{ and} \\ \hat{\Delta}_\lambda &\equiv \left\{ -\frac{\Delta\lambda}{2} = \hat{\lambda}_{-1} < \hat{\lambda}_0 < \dots < \hat{\lambda}_{N_\lambda} = 2\pi + \frac{\Delta\lambda}{2} \right\}, \end{aligned}$$

where  $N_\lambda > 0$  is an integer and  $\Delta\lambda = 2\pi/N_\lambda$  denotes the meshsize in the  $\lambda$ -direction. The two partitions  $\Delta_\lambda$  and  $\hat{\Delta}_\lambda$  are staggered with respect to each other. The gridpoints

in  $\Delta_\lambda$  and  $\hat{\Delta}_\lambda$  are chosen so that  $\lambda_i = i\Delta\lambda$  for  $i = 0, \dots, N_\lambda$ , and  $\hat{\lambda}_i = (i+1/2)\Delta\lambda$  for  $i = -1, \dots, N_\lambda$ , respectively. Similarly, staggered partitions  $\Delta_\theta$  and  $\hat{\Delta}_\theta$  are defined in the  $\theta$ -direction by

$$\begin{aligned}\Delta_\theta &\equiv \left\{ -\frac{\pi}{2} = \theta_0 < \theta_1 < \dots < \theta_{N_\theta} = \frac{\pi}{2} \right\} \text{ and} \\ \hat{\Delta}_\theta &\equiv \left\{ -\frac{\pi}{2} - \frac{\Delta\theta}{2} = \hat{\theta}_{-1} < \hat{\theta}_0 < \dots < \hat{\theta}_{N_\theta} = \frac{\pi}{2} + \frac{\Delta\theta}{2} \right\},\end{aligned}$$

where  $N_\theta > 2$  is an integer,  $\Delta\theta = \pi/N_\theta$ ,  $\theta_j = -\pi/2 + j\Delta\theta$  for  $j = 0, \dots, N_\theta$ , and  $\hat{\theta}_j = -\pi/2 + (j+1/2)\Delta\theta$  for  $j = -1, \dots, N_\theta$ .

For each partition, consider the associated one-dimensional quadratic spline space, i.e., the space of piecewise quadratic polynomials with  $C^1$  continuity on the gridpoints of the partition. Define the model quadratic spline function  $\psi$  by

$$\psi(\lambda) = \begin{cases} \lambda^2 & 0 \leq \lambda \leq 1, \\ \lambda^2 - 3(\lambda - 1)^2 & 1 \leq \lambda \leq 2, \\ \lambda^2 - 3(\lambda - 1)^2 + 3(\lambda - 2)^2 & 2 \leq \lambda \leq 3, \\ 0 & \text{otherwise,} \end{cases}$$

and let  $\{\beta_i(\lambda) = \frac{1}{2}\psi(\frac{\lambda}{\Delta\lambda} - i + 2)\}_{i=0}^{N_\lambda+1}$  and  $\{\hat{\beta}_i(\lambda) = \frac{1}{2}\psi(\frac{\lambda}{\Delta\lambda} - i + \frac{3}{2})\}_{i=-1}^{N_\lambda+1}$  be the sets of basis functions for the one-dimensional quadratic spline approximation spaces corresponding to partitions  $\Delta_\lambda$  and  $\hat{\Delta}_\lambda$ , respectively. For the partitions  $\Delta_\theta$  and  $\hat{\Delta}_\theta$ , let  $\{\beta_j(\theta) = \frac{1}{2}\psi(\frac{\theta+\pi/2}{\Delta\theta} - j + 2)\}_{j=0}^{N_\theta+1}$  and  $\{\hat{\beta}_j(\theta) = \frac{1}{2}\psi(\frac{\theta+\pi/2}{\Delta\theta} - j + \frac{3}{2})\}_{j=-1}^{N_\theta+1}$  be the respective sets of basis functions. Figure 1 shows a diagram of the latitudinal staggered grids together with the associated basis functions. There are  $N_\lambda + 2$  basis functions associated with  $\Delta_\lambda$ ,  $N_\lambda + 3$  with  $\hat{\Delta}_\lambda$ ,  $N_\theta + 2$  with  $\Delta_\theta$ , and  $N_\theta + 3$  with  $\hat{\Delta}_\theta$ . Note that the latitudinal boundary points (i.e., the poles) are not gridpoints in  $\hat{\Delta}_\theta$ .

The target functions belong to two-dimensional approximation spaces, which are chosen to be tensor products of the associated one-dimensional approximation spaces. Discretized on a C-grid, the target functions  $U^{n+1}$ ,  $V^{n+1}$ , and  $\phi^{n+1}$  are approximated in the biquadratic spline spaces defined on the induced grid partitions  $\Delta_1 \equiv \hat{\Delta}_\lambda \times \Delta_\theta$ ,  $\Delta_2 \equiv \Delta_\lambda \times \hat{\Delta}_\theta$ , and  $\Delta_3 \equiv \Delta_\lambda \times \Delta_\theta$ , respectively, by linear combinations of the basis functions  $\{\hat{\beta}_i(\lambda)\beta_j(\theta)\}_{i=-1, j=0}^{N_\lambda+1, N_\theta+1}$ ,  $\{\beta_i(\lambda)\hat{\beta}_j(\theta)\}_{i=0, j=-1}^{N_\lambda+1, N_\theta+1}$ , and  $\{\beta_i(\lambda)\beta_j(\theta)\}_{i=0, j=0}^{N_\lambda+1, N_\theta+1}$ , respectively; i.e.,  $U_\Delta^{n+1}(\lambda, \theta) = \sum_{i=-1, j=0}^{N_\lambda+1, N_\theta+1} \mathbf{U}_{i,j}^{n+1} \hat{\beta}_i(\lambda)\beta_j(\theta)$ ,

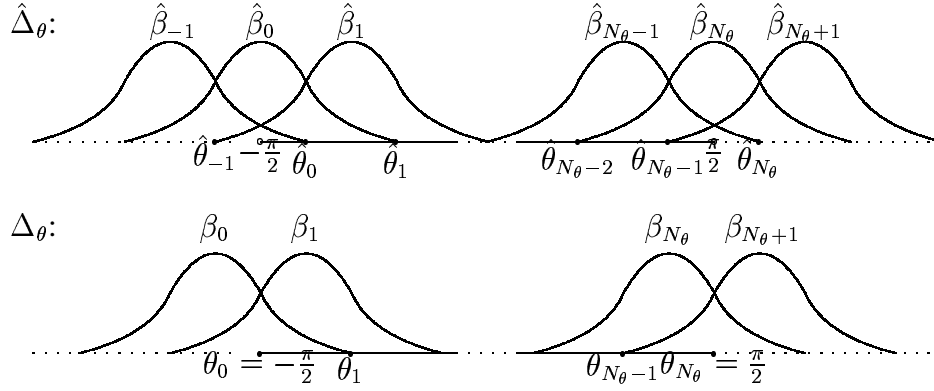


Figure 1: A diagram of the latitudinal staggered grids and associated basis functions.

$V_\Delta^{n+1}(\lambda, \theta) = \sum_{i=0, j=-1}^{N_\lambda+1, N_\theta+1} V_{i,j}^{n+1} \beta_i(\lambda) \hat{\beta}_j(\theta)$ ,  $\phi_\Delta^{n+1}(\lambda, \theta) = \sum_{i=0, j=0}^{N_\lambda+1, N_\theta+1} \Phi_{i,j}^{n+1} \beta_i(\lambda) \beta_j(\theta)$ . Furthermore, the quadratic spline representation of  $\log \phi^{n+1}$  is needed because of the  $\log \phi^{n+1}$  term in (16). Thus, we define  $\zeta^{n+1} \equiv \log \phi^{n+1}$  and approximate  $\zeta^{n+1}$  on the induced grid partition  $\Delta_3$  (same as  $\phi^{n+1}$ ) by  $\zeta_\Delta^{n+1}(\lambda, \theta) = \sum_{i=0, j=0}^{N_\lambda+1, N_\theta+1} \Gamma_{i,j}^{n+1} \beta_i(\lambda) \beta_j(\theta)$ . The coefficients  $\Gamma_{i,j}^{n+1}$  can be computed from the geopotential coefficients  $\Phi_{i,j}^{n+1}$  by first transforming  $\phi_\Delta^{n+1}$  from quadratic spline space to grid space, then computing  $\zeta_\Delta^{n+1}$  in grid space and transforming  $\zeta_\Delta^{n+1}$  to quadratic spline space to give  $\Gamma_{i,j}^{n+1}$ .

In the analysis and the implementation, the approximation spaces and the respective basis functions are adjusted so that they (and thus the approximations  $U_\Delta^{n+1}$ ,  $V_\Delta^{n+1}$ ,  $\phi_\Delta^{n+1}$ , and  $\zeta_\Delta^{n+1}$ ) satisfy the boundary conditions by construction. We explain how the latitudinal basis functions are adjusted for  $V_\Delta^{n+1}$ ; details for adjusting other basis function sets can be found in [12].

The latitudinal homogeneous Dirichlet boundary conditions on  $V_\Delta^{n+1}$  are imposed at the poles ( $V_\Delta^{n+1}(\lambda, \pm\pi/2) = 0$ ), but the poles are *not* gridpoints of  $\hat{\Delta}_\theta$ , since  $\hat{\theta}_i = -\pi/2 + (i+1/2)\Delta\theta$  for  $i = -1, \dots, N_\theta$  owing to staggering. Therefore, the incorporation of homogeneous Dirichlet boundary conditions for  $V_\Delta^{n+1}$  is non-standard and different from, e.g., that for  $U_\Delta^{n+1}$  [12]. The latitudinal components of the basis functions for  $V_\Delta^{n+1}$  are given by

$$\begin{aligned} \hat{\beta}_0^D(\theta) &= \hat{\beta}_0(\theta) - 6\hat{\beta}_{-1}(\theta), & \hat{\beta}_1^D(\theta) &= \hat{\beta}_1(\theta) - \hat{\beta}_{-1}(\theta), \\ \hat{\beta}_j^D(\theta) &= \hat{\beta}_j(\theta), & & j = 2, \dots, N_\theta - 2, \end{aligned}$$

$$\hat{\beta}_{N_\theta-1}^D(\theta) = \hat{\beta}_{N_\theta-1}(\theta) - \hat{\beta}_{N_\theta+1}(\theta), \quad \hat{\beta}_{N_\theta}^D(\theta) = \hat{\beta}_{N_\theta}(\theta) - 6\hat{\beta}_{N_\theta+1}(\theta).$$

The approximate solutions  $U_\Delta^{n+1}$ ,  $V_\Delta^{n+1}$ ,  $\phi_\Delta^{n+1}$ , and  $\zeta_\Delta^{n+1}$  are rewritten in terms of the adjusted basis functions and then substituted into (14) and (16). The inner products of the residuals of the resulting equations with each of the two-dimensional test functions are then set to zero. Thus the residuals are forced to be orthogonal to the approximation space. The resulting equations are solved by eliminating the  $U_\Delta^{n+1}$  and  $V_\Delta^{n+1}$  dependence from the system, to give rise to a discretized Helmholtz equation for  $\phi_\Delta^{n+1}$ , which is nonlinear owing to the presence of a logarithmic term. The discretized Helmholtz equation is linearized and solved using fixed-point iteration. Once  $\phi_\Delta^{n+1}$  is computed,  $U_\Delta^{n+1}$  and  $V_\Delta^{n+1}$  are updated. The details of this procedure are described in [12].

Some of the latitudinal integrals in the Galerkin procedure involve functions that may be time-dependent (e.g.,  $a(\theta)$ ) and are numerically computed at every timestep using the two-point Gauss quadrature rule. Because the quadratic spline basis functions have discontinuous second derivatives at gridpoints and because of the staggering of two grids in each dimension, the integration grid is defined to be twice as refined as the spline grid in each space dimension, in order to satisfy the smoothness assumption associated with the two-point Gauss rule.

## 4 Rossby Wave Stability

In this section, we perform a stability analysis for the QSG method applied to a simplified version of the SWEs and examine the conditions under which the discretized solutions are stable. We assume, for simplicity, an unstaggered grid and bi-periodic boundary conditions. In [17] Staniforth and Mitchell showed that, if Cartesian coordinates are used, if the discretization grid is unstaggered, and if bi-periodic boundary conditions are assumed, then the Helmholtz equation should be derived algebraically rather than analytically in order for the standard spatial discretization methods to be neutrally stable for the Rossby waves. We extend their study and demonstrate similar results in spherical coordinates.

The mathematical analysis is done on the simplified SWEs, obtained by linearizing (1)–(3) and assuming constant values for the coefficient associated with the Coriolis terms  $f + u \tan \theta / R (= f^*)$ , for  $u (= u^*)$  and  $v (= v^*)$  in the Lagrangian derivative, and for the coefficients  $\phi (= \Phi^*)$  and  $\theta (= \Theta^*)$  associated with the gradient terms. The simplified SWEs are

$$\frac{du}{dt} - f^* v + \frac{\phi_\lambda}{R \cos \Theta^*} = 0, \quad (17)$$

$$\frac{dv}{dt} + f^* u + \frac{\phi_\theta}{R} = 0, \quad (18)$$

$$\frac{d\phi}{dt} + \frac{\Phi^*}{R} \left( \frac{u_\lambda}{\cos \Theta^*} + v_\theta \right) = 0, \quad (19)$$

where

$$\frac{d}{dt} \equiv \frac{\partial}{\partial t} + \frac{u^*}{R \cos \Theta^*} \frac{\partial}{\partial \lambda} + \frac{v^*}{R} \frac{\partial}{\partial \theta}. \quad (20)$$

Equations (17)–(19) can also be obtained by linearizing (5)–(7), since, with  $\cos \Theta^*$  assumed to be constant,  $U$  and  $V$  are simply constant multiples of  $u$  and  $v$ .

*The continuous case.* We first examine the continuous problem. We assume that the solution to (17)–(19) is of the form

$$(u(\lambda, \theta, t), v(\lambda, \theta, t), \phi(\lambda, \theta, t)) = (u_0, v_0, \phi_0) e^{i(k\lambda + l\theta + \omega t)}, \quad (21)$$

where  $k$  and  $l$  are the longitudinal and latitudinal wave numbers, respectively, and  $\omega$  denotes the wave frequency. The Lagrangian frequency  $\nu$  is defined by  $\nu \equiv \frac{u^*}{R \cos \Theta^*} + \frac{v^*}{R} + \omega$ .

To compute the Lagrangian frequency of the true solution, (21) is substituted into the simplified SWEs (17)–(19). This results in a  $3 \times 3$  system of equations for  $u_0$ ,  $v_0$ , and  $\phi_0$ . Then, by setting the determinant of the system to zero, and solving for the Lagrangian frequency  $\nu$ , we obtain

$$\nu = 0, \pm \sqrt{\Phi^* \left[ \left( \frac{k}{R \cos \Theta^*} \right)^2 + \left( \frac{l}{R} \right)^2 \right] + f^{*2}}. \quad (22)$$

The first solution,  $\nu = 0$  or  $\omega = -u^*/(R \cos \Theta^*) - v^*/R$ , corresponds to the solution of interest, i.e., the Rossby waves. The other two frequencies are associated with

the gravity waves.

*Algebraic derivation of the Helmholtz equation.* We now solve the simplified SWEs (17)–(19) using the two-level SLSI method with a finite element spatial discretization scheme. We analyze the stability of the numerical solution when the Helmholtz equation is derived algebraically; i.e., we compare (22) to the Lagrangian frequency of the discretized solution when the divergence terms are eliminated *after* spatial discretization.

The one-dimensional mass and first-derivative matrices arising from the QSG method and many other discretization methods with bi-periodic boundary conditions are circulant and therefore diagonalizable by the discrete Fourier transform matrix. It follows that the longitudinal mass matrix  $P$  and the first-derivative matrix  $P_\lambda$  associated with the finite element scheme have common eigenvectors  $\vartheta_k = (e^{ikj\Delta\lambda})_{j=0}^{N_\lambda-1}$  for  $k = 0, \dots, N_\lambda - 1$ . (The explicit form for  $P$  and  $P_\lambda$  for the QSG method can be found in [12].) Let the associated eigenvalues be  $p_k$  and  $p_{\lambda k}$ , respectively. Thus, we have

$$P\vartheta_k = p_k\vartheta_k, \quad P_\lambda\vartheta_k = p_{\lambda k}\vartheta_k. \quad (23)$$

Similarly, the latitudinal mass matrix  $Q$  and the first-derivative matrix  $Q_\theta$  have common eigenvectors denoted by  $\vartheta'_l = (e^{ilj\Delta\theta})_{j=0}^{N_\theta-1}$  for  $l = 0, \dots, N_\theta - 1$ , with the associated eigenvalues denoted by  $q_l$  and  $q_{\theta l}$ , respectively. Thus, we have

$$Q\vartheta'_l = q_l\vartheta'_l, \quad Q_\theta\vartheta'_l = q_{\theta l}\vartheta'_l. \quad (24)$$

The discretized solution at time-level  $t_{n+1}$  is assumed to be of the following wave form:

$$(u_\Delta^{n+1}(\lambda, \theta), v_\Delta^{n+1}(\lambda, \theta), \phi_\Delta^{n+1}(\lambda, \theta)) = (u_0, v_0, \phi_0) e^{i(k\lambda + l\theta + \omega(n+1)\Delta t)}. \quad (25)$$

Under the assumptions of this section for constant  $f^*$ ,  $u^*$ ,  $v^*$ ,  $\Phi^*$ , and  $\Theta^*$ , the upstream function  $\tilde{\psi}^n(\lambda, \theta)$  of a function  $\psi(\lambda, \theta, t)$  is given by  $\tilde{\psi}^n(\lambda, \theta) \equiv \psi(\lambda - u^*\Delta t / (R \cos \Theta^*), \theta - v^*\Delta t / R, t_n)$ . Discretizing the simplified SWEs (17)–(19) in time using the SLSI method yields

$$\frac{u^{n+1} - \tilde{u}^n}{\Delta t} - f^* \left( \frac{v^{n+1} + \tilde{v}^n}{2} \right) + \frac{1}{R \cos \Theta^*} \left( \frac{\phi_\lambda^{n+1} + \tilde{\phi}_\lambda^n}{2} \right) = 0, \quad (26)$$

$$\frac{v^{n+1} - \tilde{v}^n}{\Delta t} + f^* \left( \frac{u^{n+1} + \tilde{u}^n}{2} \right) + \frac{1}{R} \left( \frac{\phi_\theta^{n+1} + \tilde{\phi}_\theta^n}{2} \right) = 0, \quad (27)$$

$$\frac{\phi^{n+1} - \tilde{\phi}^n}{\Delta t} + \frac{\Phi^*}{R \cos \Theta^*} \left( \frac{u_\lambda^{n+1} + \tilde{u}_\lambda^n}{2} \right) + \frac{\Phi^*}{R} \left( \frac{v_\theta^{n+1} + \tilde{v}_\theta^n}{2} \right) = 0. \quad (28)$$

Let  $E_\lambda$  and  $E_\theta$  be the quadratic spline interpolation matrices that map the vector of spline coefficients (e.g.,  $\mathbf{U}^{n+1}$ ) to the vector of function values at data points (e.g.,  $\mathbf{u}_\Delta^{n+1}$ ), where we have used the boldface type to denote vectors. The spatially discretized form of (26) can be written as

$$\begin{aligned} (P \otimes Q)(E_\lambda \otimes E_\theta)^{-1} \left( \frac{\mathbf{u}_\Delta^{n+1} - \tilde{\mathbf{u}}_\Delta^n}{\Delta t} \right) - f^*(P \otimes Q)(E_\lambda \otimes E_\theta)^{-1} \left( \frac{\mathbf{v}_\Delta^{n+1} + \tilde{\mathbf{v}}_\Delta^n}{2} \right) \\ + \frac{1}{R \cos \Theta^*} (P_\lambda \otimes Q)(E_\lambda \otimes E_\theta)^{-1} \left( \frac{\boldsymbol{\phi}_\Delta^{n+1} + \tilde{\boldsymbol{\phi}}_\Delta^n}{2} \right) = 0, \end{aligned} \quad (29)$$

where  $\otimes$  denotes the tensor product of matrices. With biperiodic boundary conditions, all matrices in parentheses in (29) commute. By pre-multiplying (29) through by  $(E_\lambda \otimes E_\theta)$  and simplifying we obtain

$$\begin{aligned} (P \otimes Q) \left( \frac{\mathbf{u}_\Delta^{n+1} - \tilde{\mathbf{u}}_\Delta^n}{\Delta t} \right) - f^*(P \otimes Q) \left( \frac{\mathbf{v}_\Delta^{n+1} + \tilde{\mathbf{v}}_\Delta^n}{2} \right) \\ + \frac{1}{R \cos \Theta^*} (P_\lambda \otimes Q) \left( \frac{\boldsymbol{\phi}_\Delta^{n+1} + \tilde{\boldsymbol{\phi}}_\Delta^n}{2} \right) = 0. \end{aligned} \quad (30)$$

Following a similar procedure, we obtain the following discretized form of (27) and (28):

$$\begin{aligned} (P \otimes Q) \left( \frac{\mathbf{v}_\Delta^{n+1} - \tilde{\mathbf{v}}_\Delta^n}{\Delta t} \right) + f^*(P \otimes Q) \left( \frac{\mathbf{u}_\Delta^{n+1} + \tilde{\mathbf{u}}_\Delta^n}{2} \right) \\ + \frac{1}{R} (P \otimes Q_\theta) \left( \frac{\boldsymbol{\phi}_\Delta^{n+1} + \tilde{\boldsymbol{\phi}}_\Delta^n}{2} \right) = 0, \end{aligned} \quad (31)$$

$$\begin{aligned} (P \otimes Q) \left( \frac{\boldsymbol{\phi}_\Delta^{n+1} - \tilde{\boldsymbol{\phi}}_\Delta^n}{\Delta t} \right) + \frac{\Phi^*}{R \cos \Theta^*} (P_\lambda \otimes Q) \left( \frac{\mathbf{u}_\Delta^{n+1} + \tilde{\mathbf{u}}_\Delta^n}{2} \right) \\ + \frac{\Phi^*}{R} (P \otimes Q_\theta) \left( \frac{\mathbf{v}_\Delta^{n+1} + \tilde{\mathbf{v}}_\Delta^n}{2} \right) = 0. \end{aligned} \quad (32)$$

Substituting the solution (25) into (30)–(32) and using (23) and (24), we obtain

$$pq \left( \frac{e^{\nu \Delta t} - 1}{\Delta t} \right) u_0 - f^* pq \left( \frac{e^{\nu \Delta t} + 1}{2} \right) v_0 + \frac{p_\lambda q}{R \cos \Theta^*} \left( \frac{e^{\nu \Delta t} + 1}{2} \right) \phi_0 = 0, \quad (33)$$

$$pq \left( \frac{e^{\nu\Delta t} - 1}{\Delta t} \right) v_0 + f^* pq \left( \frac{e^{\nu\Delta t} + 1}{2} \right) u_0 + \frac{pq\theta}{R} \left( \frac{e^{\nu\Delta t} + 1}{2} \right) \phi_0 = 0, \quad (34)$$

$$pq \left( \frac{e^{\nu\Delta t} - 1}{\Delta t} \right) \phi_0 + \frac{\Phi^*}{R \cos \Theta^*} p_{\lambda} q \left( \frac{e^{\nu\Delta t} + 1}{2} \right) u_0 + \frac{\Phi^*}{R} pq_{\theta} \left( \frac{e^{\nu\Delta t} + 1}{2} \right) v_0 = 0, \quad (35)$$

where, for notational simplicity, we have omitted the subscripts  $k$  and  $l$  from the eigenvalues  $p_k$ ,  $p_{\lambda k}$ ,  $q_l$  and  $q_{\theta l}$ . Equations (33)–(35) hold for  $k = 0, \dots, N_{\lambda} - 1$  and  $l = 0, \dots, N_{\theta} - 1$ .

Equations (33)–(35) form a  $3 \times 3$  system for  $u_0$ ,  $v_0$ , and  $\phi_0$ . By setting the determinant of the resulting system to zero, an equation for  $e^{\nu\Delta t}$  can be obtained. The roots are found to be

$$e^{\nu\Delta t} = 1, \frac{4A - B \pm 4i\sqrt{AB}}{4A + B}, \quad (36)$$

where  $A = (R \cos \Theta^* pq)^2$  and  $B = (\Delta t f^* R \cos \Theta^* pq)^2 - \Delta t^2 \Phi^* (p_{\lambda}^2 q^2 + \cos^2 \Theta^* p^2 q_{\theta}^2)$ . Since  $e^{\nu\Delta t} = 1$ , or  $\nu = 0$ , is one of the solutions, the numerical scheme is neutrally stable for the Rossby waves. The solutions for the gravity waves are also bounded since

$$|e^{\nu\Delta t}| = \left| \frac{4A - B \pm 4i\sqrt{AB}}{4A + B} \right| = 1. \quad (37)$$

Therefore, the numerical scheme is also stable for the gravitational modes. Note that the results of this analysis hold for the QSG method, the OQSC methods presented in the companion paper [11], as well as any discretization method of which the operators satisfy (23) and (24) for some  $p_k$ ,  $p_{\lambda k}$ ,  $q_l$ , and  $q_{\theta l}$ .

*Analytic derivation of the Helmholtz equation.* As noted in [12], the procedures described in Section 3 yield an approximation to a Helmholtz equation. A genuine Helmholtz equation may be derived by analytically eliminating the wind velocity dependence from the continuity equation (19) *before* spatial discretization. In the analytic derivation, we solve (26) and (27) for  $u^{n+1}$  and  $v^{n+1}$  in terms of  $\phi_{\lambda}^{n+1}$  and  $\phi_{\theta}^{n+1}$  as we did in Section 2, we obtain  $u_{\lambda}^{n+1}$  and  $v_{\theta}^{n+1}$  by taking the appropriate derivatives, and we use these expressions to eliminate the  $u_{\lambda}^{n+1}$  and  $v_{\theta}^{n+1}$  terms from (28). Then,

following procedures described for the algebraic case, we obtained a frequency equation, for which  $e^{\nu\Delta t} = 1$  is no longer a solution (see [12] for details). This result, which is consistent with [17], implies that an undesirable phase shift has been introduced into the Rossby mode. Therefore, in our formulation, the Helmholtz equation is derived algebraically to preserve the neutral stability of the Rossby waves.

## 5 Numerical Results

We now demonstrate numerically the stability of our method with respect to the Rossby waves and study its convergence behaviour. In the companion paper [11], we compare the computational cost of the QSG method to those of the linear spline Galerkin method (on which the model in [3] is based) and three quadratic spline collocation methods; we also show that when the spatial discretization is done on the C-grid, gravity waves propagate in the proper directions.

### 5.1 The Equatorial Rossby Wave

The equatorial solitary wave described by Boyd [2] is frequently used to test the stability of a numerical method for the SWEs with respect to Rossby waves [10, 13]. To use this test problem on our model, we transform Boyd's formulation, originally written in Cartesian coordinates, to spherical coordinates. We adopt Boyd's notation and let  $\phi'$  be the geopotential perturbation; that is, if we denote the reference geopotential by the constant  $\phi^*$ , then  $\phi = \phi^* + \phi'$ . The resulting nondimensional nonlinear SWEs on the equatorial  $\beta$ -plane are

$$\frac{du}{dt} - R\theta v + \frac{\phi'_\lambda}{R \cos \theta} = 0, \quad (38)$$

$$\frac{dv}{dt} + R\theta u + \frac{\phi'_\theta}{R} = 0, \quad (39)$$

$$\frac{d}{dt} \log(\phi^* + \phi') + \frac{1}{R \cos \theta} [u_\lambda + (v \cos \theta)_\theta] = 0. \quad (40)$$

The above equations are integrated with the following initial conditions

$$u(\lambda, \theta, 0) = \eta(R\lambda) \frac{-9 + 6(R\theta)^2}{4} e^{-(R\theta)^2/2}, \quad (41)$$

$$v(\lambda, \theta, 0) = 2 \frac{\partial \eta(R\lambda)}{\partial \lambda} R\theta e^{-(R\theta)^2/2}, \quad (42)$$

$$\phi'(\lambda, \theta, 0) = \eta(R\lambda) \frac{3 + 6(R\theta)^2}{4} e^{-(R\theta)^2/2}, \quad (43)$$

where  $\eta(\lambda) = A \operatorname{sech}^2(B\lambda)$ ,  $A = 0.12$ , and  $B = 0.394$ . In this study, a timestep of  $\Delta t = 0.05$  non-dimensional units (approximately two hours in simulated time) is used. Experiments are conducted with grids of sizes  $N \times N$ , with  $N = 32, 64$ , and 128. Variables are staggered using the C-grid.

The equations describe an equatorial soliton which slowly propagates westward, with no change in shape. Figure 2 shows the result of a long simulation on a  $128 \times 128$  grid for 24 non-dimensional time units, which corresponds to approximately 41 days in simulated time. In our experiments, the height fields lost about 5% of their initial amplitude which traveled eastward as equatorial Kelvin waves. We believe this is because the initial conditions (41)–(43) are inexact, as suggested by Iskandarani et al. [10] and Ma [13]. The soliton propagated westward, as predicted, with little change in amplitude or phase, thereby confirming our analysis that spatial discretization with the QSG method is neutrally stable for the Rossby modes. The small amount of dispersion present can be explained as follows. With semi-Lagrangian integration, variables are needed at departure points, which are usually off-mesh points. Cubic Lagrange interpolation is used to estimate function values at departure points. Spatial interpolation causes damping and phase shift. Compared to linear or quadratic interpolation, the effects introduced by cubic interpolation are less severe. The finer the mesh, the less prominent the damping and dispersive effects should be [1, 14]. This has been confirmed in the numerical tests described in [18].

## 5.2 Convergence Tests

Since no analytical solution is known for the general form of the two-dimensional SWEs (5)–(7), we introduce into the equations forcing terms constructed in such a way that an analytical solution is known a priori. The modified SWEs are

$$\frac{dU}{dt} - fV + \frac{\phi_\lambda}{R^2} = F_u, \quad (44)$$

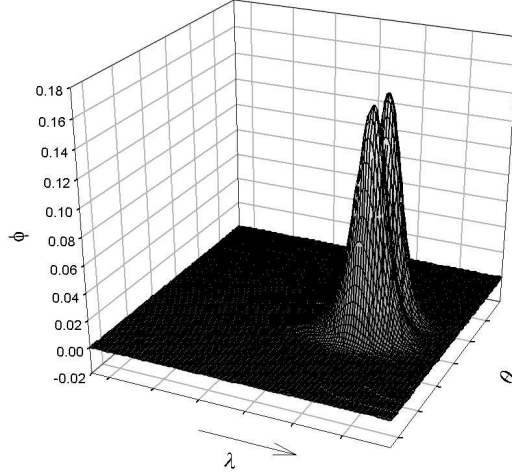


Figure 2: Simulation by the QSG method of a Rossby soliton traveling westward (in the direction indicated by the arrow, which is the direction of decreasing  $\lambda$  values) on a  $128 \times 128$  grid for 24 time units (approximately 41 days).

$$\frac{dV}{dt} + fU + \frac{\cos \theta}{R^2} \phi_\theta + \frac{\sin \theta}{\cos^2 \theta} (U^2 + V^2) = F_v, \quad (45)$$

$$\cos \theta \frac{d}{dt} \log \phi + \left[ \frac{U_\lambda}{\cos \theta} + V_\theta \right] = F_\phi, \quad (46)$$

where  $F_u$ ,  $F_v$ , and  $F_\phi$  are known functions of  $\lambda$ ,  $\theta$ , and  $t$ , defined to yield the following solution:

$$U(\lambda, \theta, t) = \frac{u_0}{R} \left[ 1 - \exp\left(-\frac{t}{T_0}\right) \right] \cos \theta \times \left\{ \exp[-a_3(\lambda - \lambda_0 - d_0)^2 - a_3(\theta - \theta_0)^2] - \exp[-a_3(\lambda - \lambda_0 + d_0)^2 - a_3(\theta - \theta_0)^2] \right\}, \quad (47)$$

$$V(\lambda, \theta, t) = \frac{v_0}{R} \left[ 1 - \exp\left(-\frac{t}{T_0}\right) \right] \cos \theta \times \left\{ \exp[-a_3(\lambda - \lambda_0)^2 - a_3(\theta - \theta_0 - d_0)^2] - \exp[-a_3(\lambda - \lambda_0)^2 - a_3(\theta - \theta_0 + d_0)^2] \right\}. \quad (48)$$

$$\phi(\lambda, \theta, t) = \phi_0 \left\{ \exp[-a_1(\lambda - \lambda_0)^2 - a_1(\theta - \theta_0)^2] - \log_e \left( 1 + \frac{t}{T_0} \right) \exp[-a_2(\lambda - \lambda_0)^2 - a_2(\theta - \theta_0)^2] \right\}, \quad (49)$$

The above functions are designed to resemble the solutions of the original SWEs (5)–(7) when these functions are given as initial conditions. In our experiments, we set

$\phi_0 = 50 g$ ,  $u_0 = v_0 = 3/2$ ,  $T_0 = 12000$  s,  $a_1 = 10$ ,  $a_2 = 60$ ,  $a_3 = 25$ ,  $\lambda_0 = \pi$ ,  $\theta_0 = 0$ ,  $d_0 = \pi/10$ , where  $g = 9.80616 \text{ ms}^{-2}$  is the gravitational constant. The system was integrated using timesteps  $\Delta t$  of 60 s. The solution for  $\phi$  was computed at  $T = 16\frac{2}{3}$  hours and compared to the reference solution (49).

We solved the system using the linear spline Galerkin (LSG) method and the QSG method with grid sizes  $32 \times 32$ ,  $64 \times 64$ ,  $128 \times 128$ , and  $256 \times 256$ . The Arakawa C-grid was used in our discretization. The computational costs for both methods are  $\mathcal{O}(N^2)$ , and are measured for a test problem in the companion paper [11]. The convergence results are shown in Table 1, where  $N = N_\lambda = N_\theta$  is the number of subintervals in one dimension. Two error norms are computed for QSG: the local error norms at gridpoints and the global error norms, labelled “ $|e|$ ” and “ $\|e\|$ ,” respectively, in Table 1. Only the local error norms at gridpoints are shown for the LSG method, because, unlike the QSG method, the LSG method does not exhibit superconvergence at special points (i.e., the local and global errors for the LSG method are of the same order). The error norms are computed as ratios of the 2-norm of the difference between the numerical solution and the reference solution, to the 2-norm of the reference solution. These errors are found to be roughly second order for LSG, and roughly fourth order for QSG locally at gridpoints and third order globally. We estimate the convergence order of the errors by  $p \equiv -\log\left(\frac{e_1}{e_2}\right) / \log\left(\frac{N_1}{N_2}\right)$  where  $e_1$  and  $e_2$  are error norms corresponding to grid sizes  $N_1$  and  $N_2$ , respectively. The computed values for  $p$  are listed in the columns labelled “ $p$ ” in Table 1.

Table 1: Observed errors and respective orders of convergence for the QSG and LSG methods with various spatial grid sizes.

$N$	QSG				LSG	
	$ e $	$p$	$\ e\ $	$p$	$ e $	$p$
32	1.756e-1	—	1.832e-1	—	2.486e-1	—
64	1.154e-2	3.93	2.322e-2	2.98	6.906e-2	1.85
128	8.779e-4	3.72	3.498e-3	2.86	1.887e-2	1.87
256	7.175e-5	3.61	4.375e-4	2.87	4.917e-3	1.94

## 6 Remarks

Spatial discretization schemes commonly used in meteorological applications are currently limited to spectral methods or low-order finite difference/finite element methods [4, 5, 9, 19, 20]. Spectral methods, which yield high-order solutions, give rise to dense matrices, therefore their parallel implementation is not scalable. In contrast, finite element methods, which give rise to sparse matrices (thus fewer global communications), have more potential for parallelism and give rise to reasonably scalable parallel implementations. Therefore, high-order finite element methods seem to be a viable alternative to spectral methods. In this paper, we present a method that combines the two-level SLSI time integration method and the QSG method for solving the SWEs on the sphere. We regard this method as a step towards high-order finite element methods that may be more efficient than spectral methods for solving partial differential equations on the sphere. A worthwhile challenge is the extension of the techniques presented in this paper and the companion paper [11] for quadratic spline collocation methods to higher-order spline methods. Such methods may yield solutions with accuracy comparable to spectral methods, but for which the specification of boundary conditions that are consistent with the actual behavior of the physical processes may be more difficult.

## References

- [1] J. R. Bates and A. McDonald. Multiply-upstream, semi-Lagrangian advection schemes: analysis and application to a multi-level primitive equation model. *Mon. Wea. Rev.*, 110:1831–1842, December 1982.
- [2] J. P. Boyd. Equatorial solitary waves. Part I: Rossby solitons. *J. Phys. Oceanogr.*, 10:1699–1717, November 1980.
- [3] J. Côté. Variable resolution techniques for weather prediction. *Meteorol. Atmos. Phys.*, 63:31–38, 1997.

- [4] J. Côté, J.-G. Desmarais, S. Gravel, A. Méthot, A. Patoine, M. Roch, and A. Staniforth. The operational CMC-MRB Global Environment Multiscale (GEM) model. Part II: Results. *Mon. Wea. Rev.*, 126:1397–1416, June 1998.
- [5] J. Côté, S. Gravel, A. Méthot, A. Patoine, M. Roch, and A. Staniforth. The operational CMC-MRB Global Environmental Multiscale (GEM) model. Part I: Design considerations and formulation. *Mon. Wea. Rev.*, 126:1373–1395, June 1998.
- [6] J. Côté and A. Staniforth. A two-time-level semi-Lagrangian semi-implicit scheme for spectral models. *Mon. Wea. Rev.*, 116:2003–2012, October 1988.
- [7] J. Côté and A. Staniforth. An accurate and efficient finite-element global model of the shallow water equations. *Mon. Wea. Rev.*, 118:2707–2717, December 1990.
- [8] G. J. Haltiner and R. T. Williams. *Numerical Prediction and Dynamic Meteorology*. John Wiley and Sons, 1980.
- [9] M. Hortal. Aspects of the numerics of the ECMWF model. In *Proceedings of a seminar held at ECMWF on recent developments in numerical methods for atmospheric modelings*, pages 127–143, 1999.
- [10] M. Iskandarani, D. B. Haidvogel, and J. P. Boyd. A staggered spectral element model with application to the ocean shallow water equations. *Int. J. Numer. Methods Fluids*, 20:393–414, 1995.
- [11] A. T. Layton, C. C. Christara, and K. R. Jackson. Optimal quadratic spline collocation methods for the shallow water equations on the sphere. Submitted to *Mathematics and Computers in Simulation*, 2002.
- [12] A. T. Layton, C. C. Christara, and K. R. Jackson. Quadratic spline Galerkin method for the shallow water equations on the sphere. Technical report, Department of Computer Science, University of Toronto, 2004.
- [13] H. Ma. A spectral element basin model for the shallow water equations. *J. Comput. Phys.*, 109:133–149, 1992.

- [14] A. McDonald. Accuracy of multiply-upstream, semi-Lagrangian advective schemes. *Mon. Wea. Rev.*, 112:1267–1275, June 1984.
- [15] A. Robert. A semi-Lagrangian, semi-implicit numerical integration scheme for the primitive meteorological equations. *Atmos.-Ocean*, 19:35–46, 1981.
- [16] A. Staniforth and J. Côté. Semi-Lagrangian integration schemes for atmospheric models – a review. *Mon. Wea. Rev.*, 119:2206–2223, September 1991.
- [17] A. Staniforth and H. Mitchell. A semi-implicit finite-element barotropic model. *Mon. Wea. Rev.*, 105:154–169, February 1977.
- [18] A. W. Tam. High-order spatial discretization methods for the shallow water equations. <http://www.cs.toronto.edu/pub/reports/na/tam-01-phd.ps.Z>, Ph.D. Thesis, Department of Computer Science, University of Toronto, Toronto, Ontario, Canada, February 2001.
- [19] D. L. Williamson and J. G. Olson. Climate simulations with a semi-Lagrangian version of the NCAR Community Climate Model. *Mon. Wea. Rev.*, 122:1594–1610, July 1994.
- [20] D. L. Williamson, J. G. Olson, and B. A. Boville. A comparison of semi-Lagrangian and Eulerian tropical climate simulations. *Mon. Wea. Rev.*, 126:1001–1012, April 1998.